Vibration Analysis of Brushless Doubly Fed Machines in the Presence of Rotor Eccentricity

Salman Abdi, Ehsan Abdi, *Senior Member, IEEE*, Hamid Toshani, and Richard McMahon

***Abstract*— In this work, an analytical study has been performed on the Brushless Doubly Fed Machine's (BDFM) vibration due to the interaction of its fundamental magnetic fields, exerting bending forces in the back iron. The effects of rotor eccentricity on exacerbating the machine's vibration have been considered by assessing the stator back iron displacement function in the presence of rotor eccentricity. Finite element analysis is carried out for a 250 kW BDFM built in frame size D400 to validate the analytical methods. The stator back iron displacement is determined for an ideally-constructed machine as well as when the rotor has static and dynamic eccentricity. In addition, the prototype BDFM was tested at different operating conditions in order to examine its noise and vibration levels. A set of measurements was conducted to assess the main vibration component frequencies developed by the machine at different rotor speeds. It is shown that the main vibration components are created by bending set-up in the back iron, rotor eccentricity, and the components with time and space harmonic natures. The results obtained from finite element analysis and experimentally agree with the analytical theory of BDFM vibration.**

***Index Terms*-- Brushless Doubly Fed Machine (BDFM); Vibration analysis; Rotor eccentricity; Beam theory; Time harmonics; Space harmonics; Rotor speed ripples; Finite element analysis.**

I. INTRODUCTION

THE Brushless Doubly Fed Machine (BDFM) is a variable speed generator or motor, which in recent years has been investigated as a possible replacement for the Doubly-Fed Induction Generator (DFIG) [1], currently used in majority of large wind turbines. Similar to the DFIG concept, a BDFM allows variable speed operation using a variable voltage, variable frequency (VVVF) converter rated at only a fraction (30-50%) of the generator rating [2], [3], but it also benefits from the fact that it does not require any brush gear, eliminating this source of failure and reducing machine maintenance, which is the key advantage of the machine [4]. The BDFM also shares with the DFIG the ability to control the reactive power flow through the machine.

To date, several large BDFMs have been manufactured, for instance in China with a 200 kW machine [5], in Brazil with the design of a 75 kW machine [6], and in the UK with the largest BDFM ever reported. The later was designed and built in a frame size D400 and tested by the authors and some aspects of the machine's performance were reported in [7] and [8]. However, to achieve successful large scale BDFMs for wind generation application with competitive design and performance specifications over its counterparts, it is essential to improve the machine design including the vibration and acoustic noise characteristics.

The BDFM is operated with one of its windings, called the power winding (PW), connected directly to the 3-phase grid. The other winding, called the control winding (CW), may be either open circuited or short-circuited, thus operating similar to induction machines, but at two different speeds [9]. However, the desirable mode of operation for a BDFM is the 'synchronous mode' in which the control winding is connected to a variable voltage variable frequency converter as shown in Fig. 1 [7]. The machine's operating point is set as with a standard synchronous machine, but by adjusting the control winding frequency this operation can be at any rotor speed, leading to variable speed generator or drive operation [10].

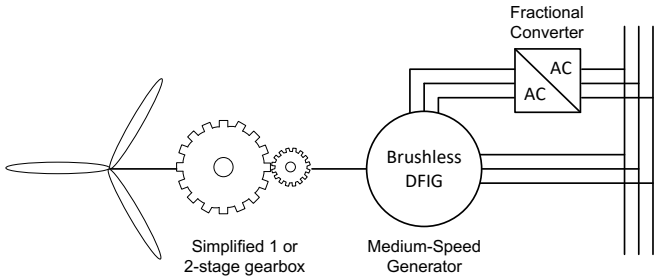

Fig. 1. A schematic of the wind turbine drive train with a BDFM as generator.

The magnetic fields in an induction machine exert significant forces on the machine's stator and rotor iron parts. Such forces can result in displacements and can be observed in the form of vibration and noise in the machine. In addition, because the BDFM has two main field components with different frequencies and pole numbers resulted from two stator windings, the vibration pattern is more complex in the BDFM than in the induction machine.

The presence of rotor eccentricity further increases the iron displacements and hence vibration levels by essentially modulating the magnetic fields produced by the stator windings and thus introducing further harmonic components [11]. Similar problem has been reported for other two-field electrical machines, such as dual stator induction machine [12]. In this work, an analytical study is conducted on the BDFM's modes of vibration caused by the interaction of its fundamental magnetic fields exerting bending forces in the back iron. The effects of rotor eccentricity, including both static and dynamic eccentricities, on exacerbating the machine's vibration are taken into account. Finite element (FE) analysis was carried out for a large-scale BDFM built in frame size D400 to validate the analytical methods. The FE models were validated by the

experimental data obtained from flux measurements of stator teeth and back iron. The stator back iron displacement is then determined for an ideally-constructed machine as well as when the rotor has static and dynamic eccentricity. The prototype BDFM was also tested at different operating conditions in order to examine its noise and vibration levels. A set of measurements was conducted to assess the main vibration frequencies at different rotor speeds.

II. Previous works on BDFM vibration

There are only few studies carried out on the vibration analysis of BDFMs. Logan et. al. [13] derived equations for vibration components magnitudes generated by the PW and CW magnetic fields as functions of air-gap flux density, pole numbers and machine dimensions. In that study however, the effects of field harmonics and eccentricity were neglected. Abdi et. al. in [14] proposed a new parallel winding design for the stator PW and CW to mitigate the vibration level in the presence of rotor eccentricity. Analytical and experimental analysis of the BDFM vibration were performed in [15] noting that the vibration amplitude may be decreased if special attention is given to the choice of loops number in the rotor cage, number of power and control windings poles and careful design of the stator core. Dorrell et. al. in [16] proposed a number of rotor designs with suitable stator pole pair combinations in order to improve the BDFM design by reducing the unbalanced magnetic pull (UMP).

In order to minimise the magnetising currents in induction type machines, it is essential to construct the machine with shortest practical air gap. However, these induction machines experience strong magnetic fields across the air gap, which can cause considerable forces exerted on the iron parts of the machine. These can ultimately lead to time-varying displacements on the machine's surface and hence transmit noise to the surrounding air.

The UMP is an undesirable characteristic in dual stator machines by which vibrations and acoustic noise can be produced. It was shown in [16] that UMP occurs when the stator windings pole-pair numbers differ by one, so this vibration source can be avoided by careful stator winding design. However, it was shown in [11, 14] that another source of vibration known as 'bending set-up in the back iron' occurs in all BDFMs irrespective of pole-pair number combinations causing displacements of stator back iron and leading to bending mode vibration in the machine.

It was shown in [13] that the dominant term in the calculation of displacements in a BDFM is related to the difference of stator pole pair numbers p_1-p_2 and angular frequencies ω_1-ω_2. This term essentially represents the existence of two fundamental field components in the machine generated by stator windings with different frequencies and pole numbers. It was also shown that the vibration component with angular frequency ω_1-ω_2 has the greatest contribution in the vibration of an ideally constructed BDFM.

As with the induction machine, the eccentricity of the rotor further modulates the field patterns, and therefore increases vibration and noise levels in the machine [17]; however, these effects are not straightforward to precisely determine through analytical calculations. Nevertheless, it will be shown in this paper that in BDFMs with static and dynamic eccentricities, vibration components at angular frequencies of ω_r, ω_1-ω_2 and ω_1-ω_2±ω_r are developed. The effects of eccentricity in the vibration spectrum are also discussed in section III.

There are other important factors that can contribute to the vibration and noise in the BDFM, such as the presence of time harmonics in stator and rotor winding currents, air gap magnetic field space harmonics, and the dynamics of the mechanical system (including natural frequencies of various components). These effects are present in the experimental results shown in section V, but their analytical investigation is outside the scope of this paper.

III. Magnetic forces and resulting displacements

A. Perfectly constructed BDFM:

As mentioned in Section II, vibration caused by bending set-up in the back iron is occurred in BDFMs irrespective of pole pair number combinations causing stator back iron displacement and leading to bending mode vibration in the BDFM.

The magnetic field in a BDFM air gap comprises two fundamental field components, one with $2p_1$ poles and the mean absolute flux density of $\bar{B}_1$ rotating at ω_1 rad/s, and another with $2p_2$ poles and $\bar{B}_2$ flux density rotating at ω_2. The net flux density is essentially the superposition of the above two field components and can be expressed as a function of time and space angle [18]:

$$B(\theta,t)=\frac{\pi}{2}[\bar{B}_1\cos(p_1\theta+\omega_1 t+\phi_1)+\bar{B}_2\cos(p_2\theta+\omega_2 t+\phi_2)] \quad (1)$$

where ω_1 and ω_2 are the frequencies of the two stator supplies, and ϕ_1 and ϕ_2 are phase angles. In (1) any harmonic field components generated by saturation, rotor structure, slotting, and rotor eccentricity are ignored.

In [13] a theoretical analysis of vibration patterns in the BDFM was proposed using beam theory as described for the induction machine by, for example, Alger [19]. Generally, this assumes that transverse deflections dominate shear deflections and that the underlying longitudinal strains are small, so that changes in curvature can be directly related to the bending moment on a given cross-section in a linear fashion [13]. Using this method, the forces exerted by the magnetic field are calculated and the resulting displacement of the iron is determined from the procedure illustrated in Fig. 2. The magnitudes of the main vibration components as function of the machine dimensions and pole numbers can then be obtained. The algebraic expression of vibration components gives an insight on how they may be changed to reduce vibration during the design of BDFMs and therefore having an analytical expression of the vibration pattern is important for the BDFM design optimisation.

Based on the above approach, the resulting displacement in the stator back iron from the exerted magnetic force produced

by the air gap magnetic field of (1) can be calculated as [14]:

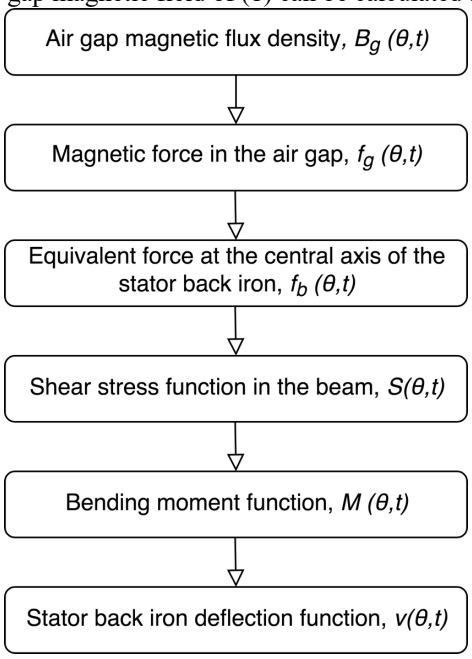

Fig. 2. A block diagram showing how stator back iron deflection is obtained using air gap flux density waveform [13].

$$v(\theta,t) = -K_v\left[\frac{1}{((2p_1)^2-1)^2}\bar{B}_1^2\cos(2p_1\theta+2\omega_1 t+2\phi_1)+\frac{1}{((2p_2)^2-1)^2}\bar{B}_2^2\cos(2p_2\theta+2\omega_2 t+2\phi_2)+\frac{2}{((p_1-p_2)^2-1)^2}\bar{B}_1\bar{B}_2\cos((p_1-p_2)\theta+(\omega_1-\omega_2)t+(\phi_1-\phi_2))+\frac{2}{((p_1+p_2)^2-1)^2}\bar{B}_1\bar{B}_2\cos((p_1+p_2)\theta+(\omega_1+\omega_2)t+(\phi_1+\phi_2))\right] \quad (2)$$

K_v is dependent on material properties and machine geometry and expressed as [13]:

$$K_v = \frac{3D_a D_c^3\pi^2}{64E_{ym}\mu_0 y_c^3} \quad (3)$$

where D_a is the air gap diameter, D_c is the median diameter of the stator back iron, y_c is the back iron depth and E_{ym} is the Young's modulus of the material. Hence, K_v is constant for a particular BDFM. The full derivation of (2) can be found in [13]. Equation (2) comprises four terms, the first two of which are single field components, as would be expected in an induction machine. The latter two terms are dependent on the difference and sum of the pole pairs, respectively. Since each term is inversely proportional to the fourth power of the pole pairs, the term that includes the difference of pole pairs, i.e. the third term with angular frequency of $\omega_1-\omega_2$, can become relatively large in BDFMs with a small difference between power and control winding pole pairs. This will be investigated experimentally in Section V.

B. BDFM with rotor eccentricity:

The previous section showed that a perfectly constructed BDFM experiences vibration modes in addition to those that would appear in an equivalent induction machine because of the interaction between two stator fields. In this section, the effect of rotor eccentricity is studied as a source of noise and vibration.

Rotor and stator eccentricity can essentially introduce additional components of flux with different pole numbers from those of the windings. Two types of eccentricity are considered in this analysis: static eccentricity where the central axes of the stator bore and the rotor shaft are offset, and dynamic eccentricity where the centre axis of rotor lamination stack is offset from the centre axis of rotor shaft. The air gap length as a result of eccentricity is:

$$g(\theta,t) = g_0 - g_s\cos(\theta+\phi_s) - g_d\cos(\theta+\omega_r t+\phi_d) \quad (4)$$

where g_0 is the average air gap length, g_s and g_d are the amplitude of the static and dynamic eccentricity components respectively, and ω_r is the rotor angular velocity. ϕ_s and ϕ_d are arbitrary angles relative to the stator reference axis. The magnetic flux density in the air gap as a result of the surface magnetizing current density $J_m(\theta,t)$ may be derived from the Ampere's law as:

$$B(\theta,t) = \mu_0 g^{-1}(\theta,t)\frac{D_a}{2}\int J_m(\theta,t)d\theta \quad (5)$$

where the MMF drops across the iron parts of the magnetic path are neglected. The inverse of air gap function in (4) can be expressed using Fourier series as:

$$g^{-1}(\theta,t) = g_0^{-1} + g_{s1}^{-1}\cos(\theta+\phi_{s1}) + g_{d1}^{-1}\cos(\theta+\omega_r t+\phi_{d1}) + \cdots = g_0^{-1}[1 + d_{s1}\cos(\theta+\phi_{s1}) + d_{d1}\cos(\theta+\omega_r t+\phi_{d1}) + \cdots] \quad (6)$$

where d_{s1} and d_{d1} are the static and dynamic eccentricity coefficients, respectively. Given these coefficients are generally very small, d_{s1} and d_{d1} may be approximated to g_s/g_0 and g_d/g_0, respectively [20].

The BDFM magnetizing current density contains p_1 pole pair PW and p_2 pole pair CW components:

$$J_m(\theta,t) = \hat{J}_{m1}\cos(p_1\theta+\omega_1 t+\phi_1) + \hat{J}_{m2}\cos(p_2\theta+\omega_2 t+\phi_2) \quad (7)$$

After substituting (6) and (7) into (5), the components of the flux are shown in Table I, where

$$\bar{B}_i = \frac{D_a}{\pi}\frac{g_0^{-1}\mu_0}{p_i}\hat{J}_{mi} \quad (8)$$

Consequently, the displacement function of the stator back iron in the presence of rotor eccentricity can be derived from the procedure described in Fig. 2. Essentially, the exerted magnetic force produced by the air gap magnetic field components of (8) can be obtained from a series of integrations in order to derive the resultant back iron displacement. The displacement components that arise are summarized in Table II, neglecting those containing the product of two or more eccentricity coefficients (e.g. $d_{s1}.d_{s2}$), which are relatively smaller than other terms. The magnitudes of displacement components given in Table II include the constant K_v given in (3). The first four components given in rows 1-4 in Table II are also present in the analysis of displacements for a perfectly constructed BDFM given in (2). The remaining components (5-24 in Table II) are created from eccentricities. As previously

noted, the displacement terms have magnitudes inversely proportional to the fourth power of the pole-pairs and thus it is those with low number of pole pairs that make significant contribution in the machine vibration.

TABLE I
AIR GAP MAGNETIC FLUX DENSITY COMPONENTS IN THE PRESENCE OF ROTOR ECCENTRICITY

i	Magnitude	Pole-pairs	Frequency	Phase
1	$\bar{B}_1$	P_1	ω_1	ϕ_1
2	$\bar{B}_2$	P_2	ω_2	ϕ_2
3	$\bar{B}_1 d'_{s1}/2$	P_1-1	ω_1	$\phi_1-\phi_{s1}$
4	$\bar{B}_1 d'_{s1}/2$	P_1+1	ω_1	$\phi_1+\phi_{s1}$
5	$\bar{B}_2 d'_{s1}/2$	P_2-1	ω_2	$\phi_2-\phi_{s1}$
6	$\bar{B}_2 d'_{s1}/2$	P_2+1	ω_2	$\phi_2+\phi_{s1}$
7	$\bar{B}_1 d'_{d1}/2$	P_1-1	$\omega_1-\omega_r$	$\phi_1-\phi_{d1}$
8	$\bar{B}_1 d'_{d1}/2$	P_1+1	$\omega_1+\omega_r$	$\phi_1+\phi_{d1}$
9	$\bar{B}_2 d'_{d1}/2$	P_2-1	$\omega_2-\omega_r$	$\phi_2-\phi_{d1}$
10	$\bar{B}_2 d'_{d1}/2$	P_1+1	$\omega_2+\omega_r$	$\phi_2+\phi_{d1}$

In a 2/4 pole pair machine, as for the D400 BDFM, there are six components with a single pole pair waveform (i.e. comps. 5, 6, 12, 15, 16 and 22 in Table II) in addition to the main displacement component present in the ideal machine analysis (comp. 3 in Table II), that together give the following approximation for the back iron displacement:

$$\begin{aligned} v(\theta,t) = 2K_V \Big[& \bar{B}_1\bar{B}_2\cos\big(\theta+(\omega_1-\omega_2)t+(\phi_1-\phi_2)\big) \\ & + d_{s1}(\bar{B}_1^2+\bar{B}_2^2)cos(\theta+\phi_{s1}) \\ & + \frac{d_{s1}}{16}\bar{B}_1\bar{B}_2\cos\big(2\theta+(\omega_1-\omega_2)t+(\phi_1-\phi_2+\phi_{s1})\big) \\ & + d_{d1}(\bar{B}_1^2+\bar{B}_2^2)cos(\theta+\omega_r t+\phi_{d1}) \\ & + \frac{d_{d1}}{16}\bar{B}_1\bar{B}_2\cos\big(2\theta+(\omega_1-\omega_2+\omega_r)t \\ & + (\phi_1-\phi_2+\phi_{d1})\big)\Big] \end{aligned} \quad (9)$$

TABLE II
DISPLACEMENTS COMPONENTS IN THE PRESENCE OF ROTOR ECCENTRICITY

Comp	Pole-pair Number	Frequency	Displacements Wave Magnitude
1	$2p_1$	$2\omega_1$	$K_v\bar{B}_1^2/(2p_1)^4$
2	$2p_2$	$2\omega_2$	$K_v\bar{B}_2^2/(2p_2)^4$
3	p_1-p_2	$\omega_1-\omega_2$	$K_v 2\bar{B}_1\bar{B}_2/(p_1-p_2)^4$
4	p_1+p_2	$\omega_1+\omega_2$	$K_v 2\bar{B}_1\bar{B}_2/(p_1+p_2)^4$
5	1	0	$K_v 2d_{s1}\bar{B}_1^2$
6	1	0	$K_v 2d_{s1}\bar{B}_2^2$
7	$2p_1-1$	$2\omega_1$	$K_v d_{s1}\bar{B}_1^2/(2p_1-1)^4$
8	$2p_1+1$	$2\omega_1$	$K_v d_{s1}\bar{B}_1^2/(2p_1+1)^4$
9	$2p_2-1$	$2\omega_2$	$K_v d_{s1}\bar{B}_2^2/(2p_2-1)^4$
10	$2p_2+1$	$2\omega_2$	$K_v d_{s1}\bar{B}_2^2/(2p_2+1)^4$
11	p_1-p_2-1	$\omega_1-\omega_2$	$K_v 2d_{s1}\bar{B}_1\bar{B}_2/(p_1-p_2-1)^4$
12	p_1-p_2+1	$\omega_1-\omega_2$	$K_v 2d_{s1}\bar{B}_1\bar{B}_2/(p_1-p_2+1)^4$
13	p_1+p_2-1	$\omega_1+\omega_2$	$K_v 2d_{s1}\bar{B}_1\bar{B}_2/(p_1+p_2-1)^4$
14	p_1+p_2+1	$\omega_1+\omega_2$	$K_v 2d_{s1}\bar{B}_1\bar{B}_2/(p_1+p_2+1)^4$
15	1	ω_r	$K_v 2d_{d1}\bar{B}_1^2$
16	1	ω_r	$K_v 2d_{d1}\bar{B}_2^2$
17	$2p_1-1$	$2\omega_1-\omega_r$	$K_v d_{d1}\bar{B}_1^2/(2p_1-1)^4$
18	$2p_1+1$	$2\omega_1+\omega_r$	$K_v d_{d1}\bar{B}_1^2/(2p_1+1)^4$
19	$2p_2-1$	$2\omega_2-\omega_r$	$K_v d_{d1}\bar{B}_2^2/(2p_2-1)^4$
20	$2p_2+1$	$2\omega_2+\omega_r$	$K_v d_{d1}\bar{B}_2^2/(2p_2+1)^4$
21	p_1-p_2-1	$\omega_1-\omega_2-\omega_r$	$K_v 2d_{d1}\bar{B}_1\bar{B}_2/(p_1-p_2-1)^4$
22	p_1-p_2+1	$\omega_1-\omega_2+\omega_r$	$K_v 2d_{d1}\bar{B}_1\bar{B}_2/(p_1-p_2+1)^4$
23	p_1+p_2-1	$\omega_1+\omega_2-\omega_r$	$K_v 2d_{d1}\bar{B}_1\bar{B}_2/(p_1+p_2-1)^4$
24	p_1+p_2+1	$\omega_1+\omega_2+\omega_r$	$K_v 2d'_{d1}\bar{B}_1\bar{B}_2/(p_1+p_2+1)^4$

From (9) it can be realised that the most important vibration frequency components expected in the BDFM vibration spectrum are: ω_r, $\omega_1-\omega_2$ and $\omega_1-\omega_2\pm\omega_r$. It should be noted that the vibration component with frequency signature of $\omega_1-\omega_2$ rad/s is created due to both bending set-up in the back iron (as shown in (2)) and eccentricity (as shown in (9)). Hence, the two mechanisms superimpose but not necessarily with the same phase over the operating speed range.

IV. FINITE ELEMENT ANALYSIS OF BDFM MAGNETIC FIELDS

Table III gives details of the 250 kW BDFM used in this study. Both stator PW and CW are connected in delta. The rotor is a nested-loop design comprising six nests, each with five loops [21]. All rotor loops are terminated with a common end-ring at one end only [22].

TABLE III
SPECIFICATIONS OF THE 250 KW D400 BDFM

Frame size	400
PW pole number	4
PW rated voltage	690V at 50 Hz (delta)
PW rated current	178 A (line)
CW pole number	8
CW rated voltage	620 V at 18 Hz (delta)
CW rated current	73 A (line)
Speed range	500 rpm ± 36%
Rated torque	3670 Nm
Rated power	250 kW at 680 rpm
Air gap diameter	439 mm
Back iron depth	54 mm
Median diameter of stator back iron	636 mm
Stack length	820 mm

Finite element (FE) analysis has been widely used, for example in [23]-[26] to study UMP and its resulting vibration in electrical machines. Finite element analysis of the 250 kW BDFM was performed using the commercial software

application EFFE [26]. The model was solved as a voltage-fed problem so that simulation results can be compared directly to experimental measurements. A 2-D analysis was performed by assuming that the machine is infinitely long in the direction parallel to the shaft to reduce the computational time. The end region leakage effects were computed using the method presented in [27] and incorporated into the analysis using lumped parameters. The modelling was performed using the time-stepping method for accurate analysis.

In the synchronous mode of operation, the PW is connected directly to the grid and the CW is supplied with variable voltage at variable frequency from a converter. The implementation of BDFM synchronous operation in FE is particularly challenging because the CW excitation voltage required to set a specific load condition cannot be predetermined as the machine is not stable in open loop. Therefore, a closed-loop controller was implemented with details described in [28]. The PW and CW voltage sources used in simulations only included the fundamental frequencies and did not contain time harmonics.

In order to validate the numerical computation of magnetic fields in FE models, the stator back iron and teeth flux densities obtained by FE analysis have been compared to the same parameters measured using flux search coils. The search coils were fitted into the BDFM as shown in Fig. 3 and the results are shown in Fig. 4. The close agreement validates the use of FE modelling in obtaining the air gap magnetic fields in the BDFM, which may be subsequently used for the analysis of stator back iron displacement.

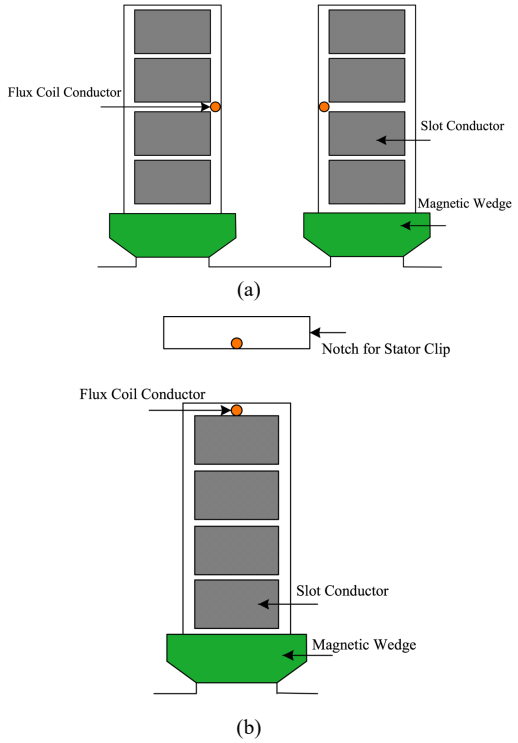

Fig. 3. Stator flux search coils fitted on to (a) stator tooth (b) stator back iron

The 250 kW BDFM is modelled in the synchronous operating mode for the two cases of ideally constructed rotor as well as when the rotor has different degrees of static and dynamic eccentricity. The flux density in the air gap is then obtained by post processing of the FE models. The stator back iron displacement can be subsequently determined using the procedure described in Fig. 2. Different levels and types of rotor eccentricity are studied. The back iron displacement for an ideally-constructed rotor as well as when the rotor has static and dynamic eccentricity are shown in Figs. 5 and 6.

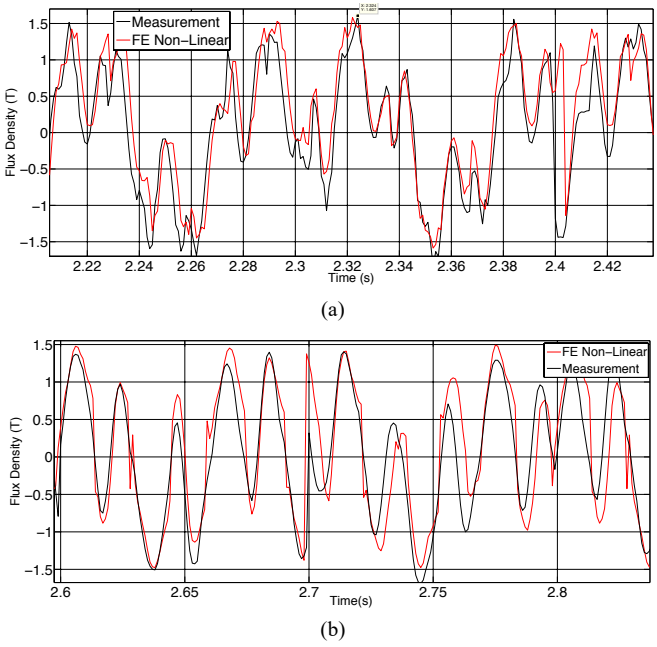

Fig. 4. Measured and predicted flux density in (a) stator tooth (b) stator back iron

From Figs. 5 and 6 the following can be concluded:

- In both static and dynamic eccentricity cases, the back iron displacement is substantially larger than when the rotor is ideally constructed.
- For the same levels of eccentricity, the severity of back iron displacement caused by rotor dynamic eccentricity is considerably higher than that of static eccentricity.
- For the case of ideally constructed rotor, the back iron displacement (green lines in Figs. 5 and 6) have 4-pole ($p_1 - p_2$ pole-pair) space distribution. This corresponds to the 3rd component of displacement function with angular frequency of $\omega_1 - \omega_2$, as predicted in Table II. It confirms the analysis of section III-A that the dominant component of back iron displacement for the ideally-constructed machine has $\omega_1 - \omega_2$ angular frequency and $p_1 - p_2$ pole pair number.
- The displacement for all other cases with static and dynamic eccentricity, have 2-pole ($p_1 - p_2 + 1$ pole-pair) space distribution. This confirms the findings of section III-B that in a BDFM with non-ideal rotor construction, the dominant displacement components have angular velocities of ω_r, $\omega_1 - \omega_2$ and $\omega_1 - \omega_2 \pm \omega_r$, which correspond to the 11th, 12th, 21st and 22nd components predicted in Table II, all with pole pair number equal to $|p_1 - p_2 \pm 1|$.

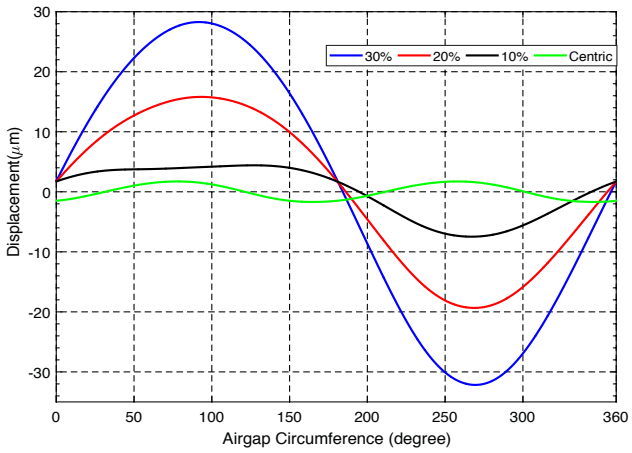

Fig. 5. Displacement in the stator back iron for ideally-constructed machine and different levels of static eccentricity.

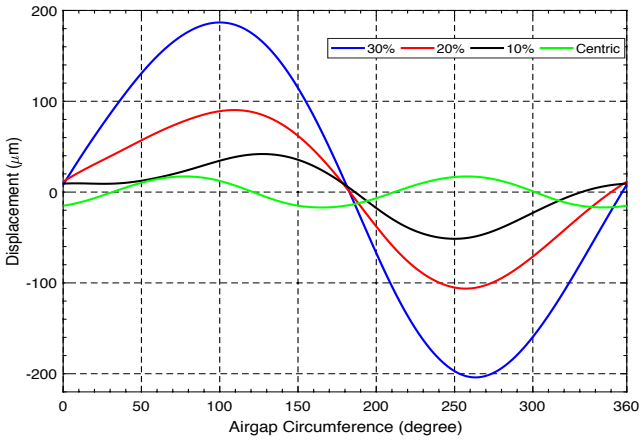

Fig. 6. Displacement in the stator back iron for ideally-constructed machine and different levels of dynamic eccentricity.

V. Experimental Assessment of Vibration in the BDFM

A. Vibration test set-up

The 250 kW BDFM is shown in Fig. 7 on the experimental rig. The machine's control system includes grid-side inverter (GSI) and machine-side inverter (MSI). The GSI was developed with an embedded control system to stabilize the DC-link and synchronize to the 690 V grid voltage. The MSI was developed to control the PW real and reactive power using a Speedgoat controller [7].

A set of measurements was conducted on the machine to validate the vibration analysis carried out in the previous section. The machine was instrumented with a number of accelerometers positioned on the bedplate, frame and terminal box of the machine, as shown in Fig. 8, and was operated in the synchronous mode of operation at a speed range of 320-620 rpm. Vibration was measured using Bruel & Kjaer 2260 instruments from the drive end of the machine with the specifications shown in Table IV. The accelerometers' signals were digitised using a data logger controlled by LabVIEW software. The fast Fourier transform of the signals were also computed using a built-in algorithm. The measured averaged root mean square (*rms*) vibration velocity over a range of operating speeds is shown in Fig. 9.

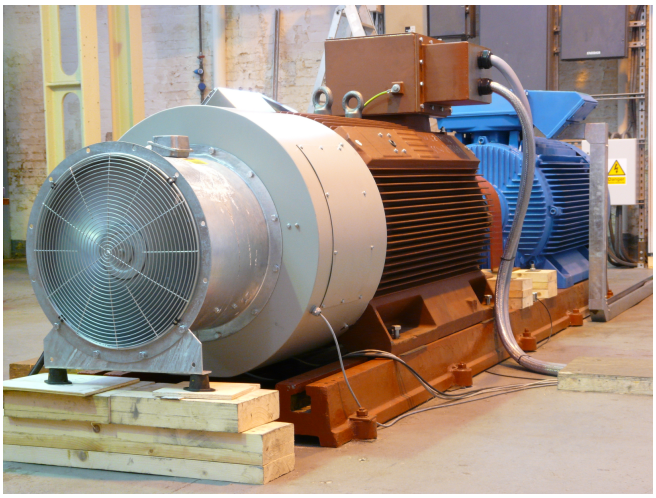

Fig. 7. 250 kW BDFM and the load machine on test rig.

As can be seen from Fig. 9, for the rotor speed between 540-680 rpm, the *rms* values of vibration velocity remain within the range of 2.87-4.01 mm/s. This is close to the standard limit, based on the ISO 10816 standard for vibration assessment of a 250 kW class M electrical machine. Nevertheless, for the operating speed range of 320-520 rpm, the measured vibration *rms* values are between 5.15 and 12.70 mm/s, which is above the tolerable limit.

TABLE IV
Specifications of the Vibration Measurement Instruments

Instrument model	Bruel & Kjaer 2260
Input type	Vibration
Full scale	117.6 m/s^2
Frequency span	312.5 Hz
Centre frequency	157.47 Hz
Frequency resolution	0.732 Hz
High pass filter	0.1 Hz
Sensitivity	845 μV/m/s^2

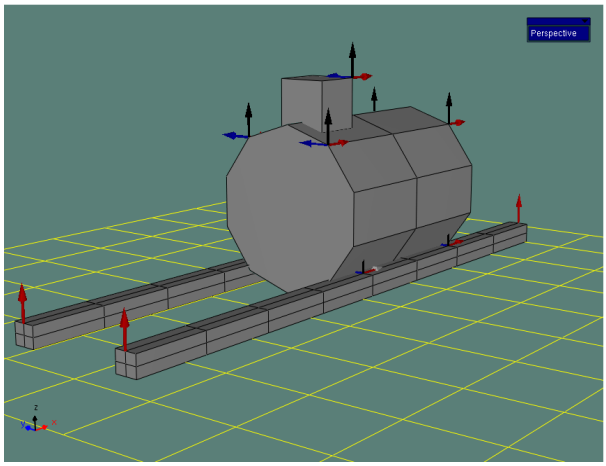

Fig. 8. Location of accelerometers on the BDFM test bed for vibration measurements.

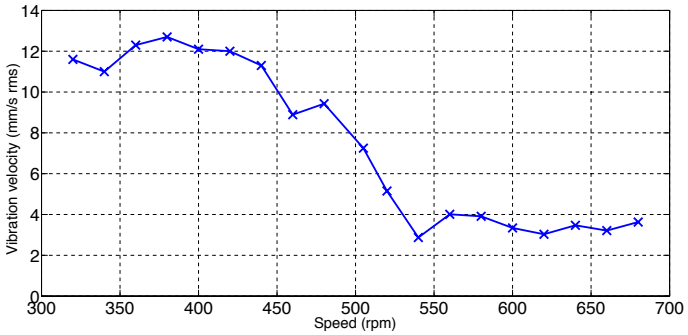

Fig. 9. Vibration velocity over the BDFM operating speed range.

B. *Measured vibration spectra*

The spectra of vibration amplitudes in dB have been obtained for the 250 kW BDFM at the operating conditions where the machine's vibration velocity is at its highest level. Fig. 10 (a) shows the vibration spectrum at the rotor speed of 440 rpm and the PW and CW supplied frequencies of 50 Hz and 6 Hz, respectively. The supply voltages were set to give magnetic loadings of 0.32 and 0.38 T for the PW and CW, respectively, in order to achieve the nominal field strength in the machine air gap.

Air gap non-uniformity was present in the prototype 250 kW BDFM, partly due to the rotor shape not being purely circular and partly due to the presence of rotor eccentricity. Experimental measurements showed that the rotor axis was off centre by approximately 15% of the air gap length. In addition, rotor whirling was observed when experimental tests were carried out at rated operating conditions, showing the presence of both static and dynamic eccentricities at normal operation.

Figure 10 (a) shows three distinct peaks at 56, 48.7 and 63.3 Hz frequencies. The 56 Hz vibration component is consistent with $\omega_1 - \omega_2$ component predicted in section III-A as the main vibration component caused by the bending set-up in the back iron of the ideally constructed BDFM. It is also consistent with $\omega_1 - \omega_2$ component predicted in section III-B as a result of rotor eccentricity. The other two frequencies, i.e. 48.7 Hz and 63.3 Hz, however, are consistent with $\omega_1 - \omega_2 \pm \omega_r$ vibration components created solely by the presence of rotor eccentricity. It is important to note that there is always a degree of rotor eccentricity present in a real machine due to manufacturing imperfection, which may cause significant vibration and noise issues in the BDFM as discussed in Section II.

Fig. 10 (b) shows the vibration spectrum at the rotor speed of 320 rpm and the PW and CW supplied frequencies of 50 Hz and 18 Hz, respectively. The main peak vibration frequencies are 68, 63 and 73.3 Hz, which correspond to $\omega_1 - \omega_2$ and $\omega_1 - \omega_2 \pm \omega_r$, similar to what was found at 440 rpm.

The time and space harmonic contents in the BDFM torque, PW and CW currents, and active powers and their contribution in the machine vibration were studied in [29], [30]. Fig. 10 also demonstrates these harmonic-driven sources of vibration, which are denoted with different colours and numbers. Table V shows different vibration mechanisms and their associated numbers and colours. These additional vibration components generated from harmonic effects can exacerbate the vibration and noise levels and therefore, special design considerations such as rotor design optimisation and use of magnetic wedges in rotor slot openings need to be employed to reduce the harmonic effects.

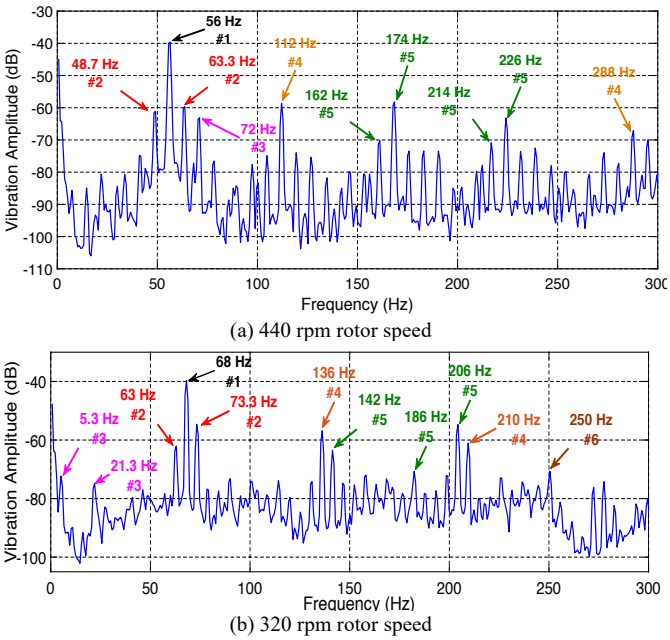

(a) 440 rpm rotor speed

(b) 320 rpm rotor speed

Fig. 10: Vibration amplitude spectrum at the machine's drive end at 0 kW (no-load), 100 kVAR, (a) 440 rpm, (b) 320 rpm.

The vibration spectrum for a range of synchronous speeds was also obtained where the output active and reactive power were kept constant at 230 kW and 98 kVAR, respectively. For each speed, the three dominant frequencies with largest magnitudes were determined and are shown in Fig. 11. The solid, dashed and dotted lines in Fig. 11 correspond to $\omega_1 - \omega_2$, $\omega_1 - \omega_2 + \omega_r$, and $\omega_1 - \omega_2 - \omega_r$, respectively.

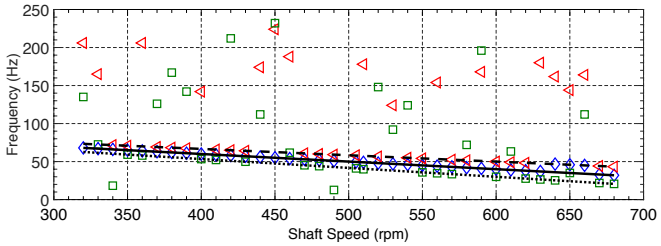

Fig. 11: Dominant frequencies in the vibration spectrum. For each speed the diamond, triangle and rectangle are the frequencies of largest, second largest and third largest components, respectively. The solid, dashed and dotted lines correspond to $\omega_1 - \omega_2$, $\omega_1 - \omega_2 + \omega_r$, and $\omega_1 - \omega_2 - \omega_r$, respectively.

As can be seen, the largest displacement component at most speeds has the frequency of $\omega_1 - \omega_2$, which corresponds to the source of vibration that includes the effects of both back iron bending set-up and rotor eccentricity. There are also reasonable correlations between the frequencies of second and third largest displacement components and the predicted rotor eccentricity vibration sources with $\omega_1 - \omega_2 + \omega_r$, and $\omega_1 - \omega_2 - \omega_r$, respectively. However, the variation in the frequency of second and third largest components seen in Fig. 11 suggests that other vibration mechanisms are taking part in the BDFM's vibration and noise patterns. These frequencies correspond mostly to the vibration mechanisms noted in Table V.

TABLE V
THE ASSOCIATED COLOUR TO EACH SOURCE OF VIBRATION FREQUENCY IN FIG. 10.

No	Vibration mechanism	Associated colour in Fig. 10
1	Bending set-up in the back iron and rotor eccentricity	Black
2	Rotor eccentricity	Red
3	Speed variation	Purple
4	Load machine's control drive	Orange
5	Space harmonics	Green
6	PW and CW time harmonics	Brown

VI. CONCLUSIONS

In this paper, various vibration mechanisms present in the BDFM's main mode of operation, the synchronous mode, were studied. It was shown that one of the main sources of vibration is created by bending set-up in the back iron, which occurs in any BDFM irrespective of pole pair combinations, causing a stator back iron displacement. It was also shown analytically that the displacement component with an angular frequency and pole-pair number of $\omega_1 - \omega_2$ and $p_1 - p_2$ (e.g. 4-pole displacement component for a 4/8 pole prototype BDFM) can become very large in BDFMs with a small difference between power and control winding pole pairs and hence is the dominant vibration component in an ideally-constructed BDFM.

In addition, it was shown that the rotor eccentricity introduces additional components of back iron displacement and results in BDFM vibration with the dominant frequencies of $\omega_1 - \omega_2$ and $\omega_1 - \omega_2 \pm \omega_r$ and pole-pair number $|p_1 - p_2 \pm 1|$ (e.g. 2-pole displacement component for a 4/8 pole BDFM). The analytical theory was validated through deriving the back iron displacement in a 250 kW BDFM from the air gap magnetic fields obtained from the finite element analysis.

A set of vibration tests were carried out on the prototype BDFM in order to assess the machine's vibration pattern. The experimental results confirmed the dominant vibration frequencies of $\omega_1 - \omega_2$ and $\omega_1 - \omega_2 \pm \omega_r$ as predicted analytically for an eccentric BDFM. A degree of air gap non-uniformity was present in the prototype machine due to the uneven air gap length caused by manufacturing tolerance as well as rotor eccentricity.

Therefore, it is essential to implement appropriate design considerations in order to mitigate the vibration and noise levels before a large-scale BDFM is constructed for wind turbine drive trains. These may include increasing the air gap length, introduction of damping in the rotor winding, introduction of damping in the stator winding with parallel paths, and isolation of the stator frame from the stator core.

VII. REFERENCES

[1] McMahon, R., Wang, X., Abdi, E., Tavner, P., Roberts, P., Jagiela, M.: ' The BDFM as a generator in wind turbines' . *Power Electronics and Motion control Conf.*, Portoroz, Slovenia, pp. 1859– 1865, 2006.

[2] M. Gholizadeh, A. Oraee, S. Tohidi, H. Oraee, R. McMahon, 'An analytical study for low voltage ride through of the brushless doubly fed induction generator during asymmetrical voltage dips', *Elsevier Renewable Energy*, Vol. 115, pp. 64-75, January 2018.

[3] Carlson, R. Voltolini, H. Runcos, F. Kuo-Peng, P. Baristela, 'Performance analysis with power factor compensation of a 75 kW brushless doubly fed induction generator prototype'. *IEEE Int. Conf. Electric Machines & Drives,* Antalya, Turkey, May 2007, vol. 2, pp. 1502– 1507

[4] Liu, H., Xu, L.: 'Design and performance analysis of a doubly excited brushless machine for wind power generator application' . *IEEE Int. Symp. Power Electronics for Distributed Generation Systems*, Hefei, China, June 2010, pp. 597– 601

[5] H. Liu and L. Xu, "Design and performance analysis of a doubly excited brushless machine for wind power generator application." *IEEE International Symposium on Power Electronics for Distributed Generation Systems*, 2010, pp. 597 – 601.

[6] R. Carlson, H. Voltolini, F. Runcos, P. Kuo-Peng, and N. Baristela, "Performance analysis with power factor compensation of a 75 kw brushless doubly fed induction generator prototype." *IEEE International Conference on Electric Machines and Drives*, 2010.

[7] E. Abdi, R. McMahon, P. Malliband, S. Shao, M. Mathekga, P. Tavner, S. Abdi, A. Oraee, T. Long, and M. Tatlow, "Performance analysis and testing of a 250 kw medium-speed brushless doubly fed induction generator," *Renewable Power Generation, IET*, vol. 7, no. 6, pp. 631 – 638, 2013.

[8] T. Long; S. Shao; P. Malliband; E. Abdi; R. A. McMahon,' Crowbarless Fault Ride-Through of the Brushless Doubly Fed Induction Generator in a Wind Turbine Under Symmetrical Voltage Dips', *IEEE Transactions on Industrial Electronics*, Vol. 60, Issue 7, 2013.

[9] T. Strous, X. Wang, H. Polinder, J. Ferreira, 'Brushless doubly fed induction machines: Magnetic field analysis', *IEEE Transactions on Magnetics*, Vol. 52, No. 11, November 2016.

[10] S. Shao, E. Abdi, R. McMahon, 'Low-cost variable speed drive based on a brushless doubly fed motor and a fractional unidirectional converter', *IEEE Transactions on Industrial Electronics,* Vol. 59, No. 1, Jan 2012.

[11] J. Li, D. Choi, and Y. Cho, 'Analysis of rotor eccentricity in switched reluctance motor with parallel winding using fem'. *IEEE Transactions on Magnetics*, vol. 45, pp. 2851 – 2854, 2009.

[12] Munoz, A.R., Lipo, T.A.: 'Dual stator winding induction machine drive', *IEEE Trans. Ind. Appl.*, 2000, 36, pp. 1369 1379.

[13] T. Logan, R. McMahon, and K. Seffen, 'Noise and vibration in brushless doubly fed machine and brushless doubly fed reluctance machine,' *IET Electric Power Applications*, vol. 7, pp. 1 – 10, 2014.

[14] S. Abdi, E. Abdi, R. McMahon, 'A Study of Unbalanced Magnetic Pull in Brushless Doubly Fed Machines' *IEEE Transactions on Energy Conversion,* vol. 30, pp. 1218 – 1227, 2015.

[15] F. Runcos, R. Carlson, N. Sadowski, P. Kuo-Peng, H. Voltolini, 'Performance and vibration analysis of a 75 kW brushless doubly fed induction generator prototype'. *IEEE Industry Applications Conference*, USA 2006.

[16] Dorrell, D. Knight, A. Betz, 'Issues with the design of brushless doubly-fed reluctance machines: unbalanced magnetic pull, skew and iron losses'. *2011 IEEE Int. Electric Machines and Drives Conf.* (IEMDC), 2011, pp. 663–668.

[17] D. Dorrell and A. Smith, 'Calculation of U.M.P in induction motors with series or parallel winding connections,' *IEEE Trans. Energy Conversion*, vol. 9, no. 2, pp. 304–310, Jul. 1994.

[18] R.A. McMahon, P. Roberts, X. Wang, P. J. Tavner' 'Performance of BDFM as generator and motor', *IET Electric Power Application*, Vol. 153, Issue 2, pp. 289-299, 2006.

[19] Alger, P.L., 'The nature of polyphase induction machines', *John Wiley & Sons*, New York, 1951.

[20] D. Dorrell, W. Thomson, S. Roach, 'Analysis of air gap flux, current and vibration signals as a function of the combination of static and dynamic airgap eccentricity in 3-phase induction motors', *IEEE Transactions on Industry Applications*, Vol 33, No. 1, January 1997.

[21] F. Barati, S. Shao, E. Abdi, H. Oraee, R. McMahon, 'Generalized vector model for the brushless doubly fed machine with a nested-loop rotor', *IEEE Transactions on Industrial Electronics*, Vol. 58, No. 6, June 2011.

[22] R. McMahon, P. Tavner, E. Abdi, P. Malliband, and D. Barker, 'Characterising brushless doubly fed machine rotors,' *IET Electric Power Applications*, vol. 7, pp. 535 – 543, 2013.

[23] A. Burakov and A. Arkkio, "Comparison of the unbalanced magnetic pull mitigation by the parallel paths in the stator and rotor windings," *IEEE Trans. Magn.*, vol. 43, no. 12, pp. 4083–4088, Dec. 2007.

[24] M. DeBortoli, S. Salon, and C. Slavik, "Effects of rotor eccentricity and parallel windings on induction machine behaviour: A study using finite element analysis," *IEEE Trans. Magn*., vol. 29, no. 2, pp. 1676–1682, Mar. 1993.

[25] D. Zarko, D. Ban, I. Vazdar, and V. Jaric, "Calculation of unbalanced magnetic pull in a salient pole synchronous generator using finite-element method and measured shaft orbit," *IEEE Transactions on Industrial Electronics*, vol. 59, no. 6, pp. 2536–2548, Jun. 2012.
[26] D. Dorrell and D. Ionel, "Radial forces and vibrations in permanent magnet and induction machines," IEEE Power Energy Soc. Gen. Meeting, 2012, pp. 1–6.
[27] S. Abdi, E. Abdi, A. Oraee, and R. McMahon, "Equivalent circuit parameters for large brushless doubly fed machines," *IEEE Transactions on Energy Conversion*, vol. 29, no. 6, pp. 706 – 715, 2014.
[28] M. Mathekga, S. Shao, T. Logan, and R. McMahon, "Implementation of a pi phase angle controller for finite element analysis of the BDFM." 6th *IET International Conference on Power Electronics, Machines and Drives (PEMD)*, Bristol, pp. 1–6, March 2012.
[29] F. Blazquez, C. Veganzones, D. Ramirez, and C. Platero, 'Characterization of the rotor magnetic field in a brushless doubly-fed induction machines,' *IEEE Trans. Energy Conversion*, vol. 24, no. 3, pp. 599–607, Sep. 2009.
[30] S. Abdi, D. Llano, E. Abdi, P. Malliband, R. McMahon, 'Experimental analysis of noise and vibration for large brushless doubly fed machines', IET The Journal of Engineering, vol. 2017, pp. 724–728, 2017.

VIII. BIOGRAPHIES

Salman Abdi received the B.Sc. degree from Ferdowsi University, Mashhad, Iran, in 2009, and the M.Sc. degree from the Sharif University of Technology, Tehran, Iran, in 2011, both in electrical engineering. He then completed the Ph.D. degree in electrical machines design and modeling from Cambridge University, Cambridge, U.K, in 2015. He is currently an Assistant Professor in Electrical Engineering at the University of East Anglia (UEA), Norwich, UK. His main research interests include electrical machines and drives for renewable power generation and automotive applications.

Ehsan Abdi (SM'12) received the B.Sc. degree from the Sharif University of Technology, Tehran, Iran, in 2002, and the M.Phil. and Ph.D. degrees, from Cambridge University, Cambridge, U.K., in 2003 and 2006, respectively, all in electrical engineering. He is currently the Managing Director of Wind Technologies Ltd., Cambridge, where he has been involved with commercial exploitation of the brushless doubly fed induction generator technology for wind power applications. He became a Senior Member of the IEEE in 2012. His main research interests include electrical machines and drives, renewable power generation, and electrical measurements and instrumentation.

Hamid Toshani received the B.S. degree in Electrical Engineering from Ferdowsi University of Mashhad, Mashhad, Iran, in 2009 and the M.Sc. degree in Control Engineering from Iran University of Science and Technology, Tehran, Iran, in 2012. He is currently a Ph.D. student majoring in Control Engineering in the Department of Electrical Engineering, Iran University of Science and Technology, Tehran, Iran. His research interests include robust control, optimization techniques and intelligent approaches in control systems.

Richard McMahon received the B.A. degree in electrical sciences and the Ph.D. degree from the University of Cambridge, Cambridge, U.K., in 1976 and 1980, respectively. Following post-doctoral work on semiconductor device processing, he became a University Lecturer in electrical engineering with the Engineering Department, University of Cambridge, in 1989, where he was a Senior Lecturer in 2000. In 2016, he joined the Warwick Manufacturing Group (WMG), University of Warwick, Coventry, U.K., as a Professor of power electronics. His current research includes electrical machines, power electronics and the electrification of transport.